Proceedings of the 2012 IFAC Workshop on Automatic
Control in Offshore Oil and Gas Production, Norwegian
University of Science and Technology, Trondheim,
Norway, May 31 - June 1, 2012

FrBT2.1

Tool-Point Control for a Redundant Heave Compensated Hydraulic Manipulator

Magnus B. Kjelland [*] **Ilya Tyapin** [*] **Geir Hovland** [*]
Michael R. Hansen [*]

[*] *University of Agder, Department of Engineering, Grimstad, Norway*
(e-mail: (magnus.b.kjelland, ilya.tyapin, geir.hovland,
michael.r.hansen)@ uia.no).

Abstract: In this paper, theoretical and experimental implementation of heave compensation on a redundant hydraulically actuated manipulator with 3-dof has been carried out. The redundancy is solved using the pseudo-inverse Jacobian method. Techniques for minimizing velocities and avoiding mechanical joint saturations is implemented in the null space joint motion. Model based feed-forward, combined with a PI-controller handles the velocity control of each joint. A time domain simulation model has been developed, experimentally verified, and used for controller parameter tuning. Model verification and experimental results are obtained while the manipulator is exposed to wave disturbances created in a dry environment by means of a Stewart platform.

Keywords: End Point Control, Active Compensation, Electro-Hydraulic Systems, Redundant Manipulators, Sensors.

1. INTRODUCTION

Heave compensation is widely used in offshore areas such as oil and gas, ship transportation and wind power systems, where disturbances from sea waves affect the motion of structures and articulated systems. Material handling machines are greatly affected by the ocean environment. Acceleration forces created by wave motion is a challenge because of their unpredictable nature as well as their size. They may attenuate nominal loads and introduce loads in new directions. In any case, they may have a substantial influence on the design of the equipment and should always be carefully considered. Heave compensation is a key factor in minimizing the effect of wave induced motion. When implemented it reduces the loads on the equipment and increase the weather windows that the equipment may operate in. For a heave compensated manipulator, the task can be to minimize the velocity of the tool point in reference to an earth fixed coordinate system. Often the tool point can be a hook that a hanging load is attached to, or it can be a gripper tool for transporting objects.

Tool point control for a non-redundant manipulator is done via the inverse kinematics. This yields either reference position or reference velocities for the actuated joints depending on the specific task. Inverse kinematic control for hydraulic/electric manipulators can be done by work from Cinkelj et al. (2010) and Kucuk and Bingul (2004).

Approaches for solving the joint position for a given tool point position for a redundant manipulator is proposed in Beiner and Mattila (1999) and Park et al. (2001). As an advantage the redundancy also gives the opportunities to optimize properties for the manipulator by controlling the null space motion of the manipulator. Work has been done

to find optimization functions that can increase performance by controlling the null space motion. An approach by Han and Chung (2007) minimizes the restoring moments.

The main contribution in this paper is the experimental verification of the well known pseudo-inverse Jacobian toolpoint control, including the null-space motion control for avoiding joint saturation, for a hydraulically actuated manipulator. Experimentation was done using a Stewart platform as a disturbance source, inducing simulated wave motion.

Fig. 1. *Experimental setup showing Stewart platform, redundant hydraulic crane and laser tracker for measuring the tool point location.*

2. TOOL POINT CONTROL

The redundant manipulator investigated in this paper is a three-bar mechanism. It consists of two rotational and one translative joint as shown in Fig. 2. Each joint is actuated by a hydraulic cylinder connected to a servo valve. The two rotational joint angles are measured using quadrature encoders. The extension of the translative joint is measured by a linear potentiometer.

2.1 Kinematics

The forward kinematics of the manipulator's tool point can be written in as:

$$\mathbf{x}_{1P} = L_1 \cos(\mathbf{q}_1) + (L_2 + \mathbf{q}_3) \cos(\mathbf{q}_1 - \mathbf{q}_2) \quad (1)$$
$$\mathbf{x}_{2P} = L_1 \sin(\mathbf{q}_1) + (L_2 + \mathbf{q}_3) \sin(\mathbf{q}_1 - \mathbf{q}_2) \quad (2)$$
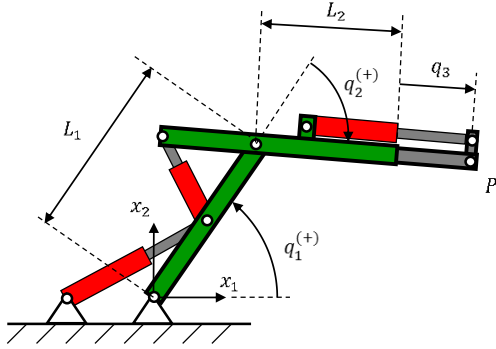

Fig. 2. *Kinematic structure of the redundant manipulator.*

The kinematics of the redundant manipulator and their time derivatives containing n links is written as follows.

$$\mathbf{x} = \mathbf{f}(\mathbf{q}) \quad (3)$$
$$\dot{\mathbf{x}} = \mathbf{J}(\mathbf{q})\dot{\mathbf{q}} \quad (4)$$

where $\mathbf{x} \in R^m (n > m)$ is the position coordinates of the end-point with m degrees of freedom, and $\dot{\mathbf{x}}$ is the end-point velocity which is normally prescribed in tracking and planned path operations. The vector $\mathbf{q} \in R^n$ is the joint position and $\dot{\mathbf{q}}$ is the joint velocity, $\mathbf{J}(\mathbf{q}) \in R^{m \times n}$ is the Jacobian matrix defined as:

$$\mathbf{J} = \frac{\partial \mathbf{f}(\mathbf{q})}{\partial \mathbf{q}} \quad (5)$$

The kinematics yield the following expression for the Jacobian entries:

$$J_{(1,1)} = -L_1 \sin(\mathbf{q}_1) - \sin(\mathbf{q}_1 - \mathbf{q}_2)(L_2 + \mathbf{q}_3)$$
$$J_{(1,2)} = \sin(\mathbf{q}_1 - \mathbf{q}_2)(L_2 + \mathbf{q}_3)$$
$$J_{(1,3)} = \cos(\mathbf{q}_1 - \mathbf{q}_2)$$
$$J_{(2,1)} = L_1 \cos(\mathbf{q}_1) + \cos(\mathbf{q}_1 - \mathbf{q}_2)(L_2 + \mathbf{q}_3)$$
$$J_{(2,2)} = -\cos(\mathbf{q}_1 - \mathbf{q}_2)(L_2 + \mathbf{q}_3)$$
$$J_{(2,3)} = \sin(\mathbf{q}_1 - \mathbf{q}_2)$$

For a non-redundant manipulator, (n = m), the relations between the joint and tool-point velocities are found by combining (4) and (5):

$$\dot{\mathbf{q}} = \mathbf{J}^{-1}\dot{\mathbf{x}} \quad (6)$$

For a redundant manipulator, however, the jacobian matrix is non-square and not invertible, hence the pseudo-inverse of the Jacobian ($\mathbf{J}^\dagger$) is used as in Whitney (1969).

$$\mathbf{J}^\dagger = \mathbf{J}^T(\mathbf{JJ}^T)^{-1} \quad (7)$$

Equation (7) defines the pseudo-inverse Jacobian which may replace $\mathbf{J}^{-1}$ in (6) yielding a new equation (8) which represents the relation between the joint and tool point velocities of the redundant manipulator.

$$\dot{\mathbf{q}} = J^\dagger(\mathbf{q})\dot{\mathbf{x}} \quad (8)$$

Computing the joint velocities according to (8) corresponds to choosing the set of joint velocities that minimizes $\frac{1}{2}\dot{\mathbf{q}}^T\dot{\mathbf{q}}$ while meeting the end-point velocity constraint. In equation (9) the weighting matrix $\mathbf{W}$ is introduced so that the redundancy is handled by minimizing $\frac{1}{2}\dot{\mathbf{q}}^T\mathbf{W}\dot{\mathbf{q}}$. This makes it possible to take into account the velocity limits of each joint. The matrix $\mathbf{W} \in R^{n \times n}$ is a positive diagonal matrix and contains a weighting of each of the joint velocities.

$$\mathbf{W} = \begin{bmatrix} W_1 & 0 & 0 \\ 0 & W_2 & 0 \\ 0 & 0 & W_3 \end{bmatrix} \quad (9)$$

$$(10)$$

In this paper the following weighting is adopted:

$$W_i = \frac{1}{(v_i^U - v_i^L)^2}, \quad i = 1..3 \quad (11)$$

where v_i^U and v_i^L are the upper and lower limit, respectively, of the velocity of the i'th joint. A joint with a low velocity range will therefore be less activated during the operation. The following expression is obtained for the weighed pseudo-inverse Jacobian:

$$\mathbf{J}_\mathbf{W}^\dagger = \mathbf{W}^{-1}\mathbf{J}^T(\mathbf{JW}^{-1}\mathbf{J}^T)^{-1} \quad (12)$$

A more general solution of (8) is presented by (13), where the weighted Pseudo-inverse Jacobian is used, see for example Siciliano (1990).

$$\dot{\mathbf{q}}_\mathbf{W} = J_\mathbf{W}^\dagger \dot{\mathbf{x}} + (\mathbf{I} - \mathbf{J}_\mathbf{W}^\dagger \mathbf{J})\dot{\mathbf{q}}_0 \quad (13)$$

Here $\mathbf{I} \in R^{n \times n}$ is the identity matrix and $\dot{\mathbf{q}}_0 \in R^n$ is an arbitrary joint velocity vector. In (13) the null space mapping is introduced. The term $(\mathbf{I} - \mathbf{J}_\mathbf{W}^\dagger \mathbf{J})\dot{\mathbf{q}}_0$ produces only a joint self-motion of the structure, but no task space motion.

A widely adopted approach is to solve the null space redundancy by optimizing the scalar cost function $h(\mathbf{q})$ using the gradient projection method, choosing $\dot{\mathbf{q}}_0$ to be the derivative of the cost function with regards to the joints, (14).

$$\dot{\mathbf{q}}_0 = \frac{\partial h}{\partial \mathbf{q}} \quad (14)$$

The cost function (15) was introduced by Ligeois (1977) and used in Pedersen et al. (2010) and Chan and Dubey (1993) before. The main goal of the cost function is to avoid mechanical joint saturation.

$$h(\mathbf{q}) = \frac{1}{3} \sum_{i=1}^{i=3} \left(\frac{\mathbf{q}_i - a_i}{a_i - y_i^U} \right)^2 \quad (15)$$

$$a_i = \frac{y_i^U + y_i^L}{2} \quad (16)$$

where y_i^U and y_i^L are the upper and lower limit, respectively, of the joint i.

2.2 Actuators

The transformation from joint velocity to cylinder velocity is:

$$\mathbf{v} = \mathbf{C}(\mathbf{q})\dot{\mathbf{q}} \qquad (17)$$

In (17) $\mathbf{v} \in R^n$ contains the cylinder velocities and $\mathbf{C} \in R^{n \times n}$ decribes the transformation that can be written as:

$$\mathbf{C}(\mathbf{q}) = \begin{bmatrix} R_1 \cos(\gamma_1) & 0 & 0 \\ 0 & R_2 \cos(\gamma_2) & 0 \\ 0 & 0 & 1 \end{bmatrix} \qquad (18)$$

The angles γ_1 and γ_2 are functions of q_1 and q_2, see figure 3
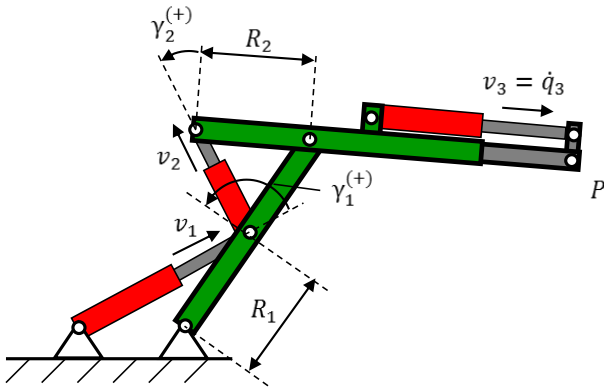
Fig. 3. *Kinematic structure for the actuation system.*

The governing steady state equation for the hydraulic actuated cylinder are described by (19-21).

$$Q_i = A_i \cdot v_i \qquad (19)$$

$$Q_i = Q_{N,i} \cdot u_i \cdot sign(\Delta p_i) \cdot \sqrt{\frac{|\Delta p_i|}{\Delta p_{N,i}}} \qquad (20)$$

$$\Delta p_i = \begin{cases} p_s - p_i, & u_i \geq 0 \\ p_i, & u_i < 0 \end{cases} \qquad (21)$$

In (19-21) $i = 1...3$ is the circuit index. Furthermore, Q is the volume flow and A is the piston area. The servo valve is modeled as a sharp edge orifice based on nominal parameters. They are the nominal volume flow Q_N that is measured at a nominal pressure drop Δp_N across the orifice with the valve fully opened. The spool travel $-1 \leq u \leq 1$ is the controlled variable of the valve. Based on the equations above it is possible to compute a spool position from the cylinder velocities if the pressure drop is known.

$$u_i = \frac{A_i \cdot v_i}{Q_{N,i}} \sqrt{\frac{\Delta p_{N,i}}{|\Delta p_i|}} \qquad (22)$$

This equation, used as a forward coupling term shown in figure 5, can in a more compact form be rewritten as:

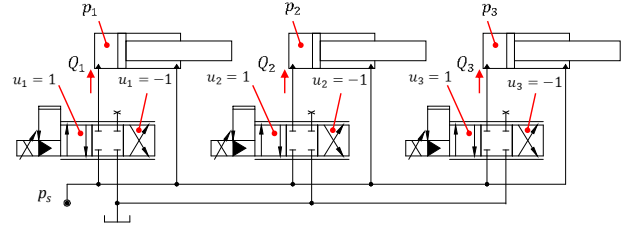$$\mathbf{u} = \mathbf{D}(\mathbf{p})\mathbf{v} \qquad (23)$$

Fig. 4. *Hydraulic diagram of the manipulator.*

2.3 Controller Structure

The motion control for the redundant manipulator is based on the pseudo-inverse Jacobian and the null-space vector. The controller generates a joint velocity reference that is given to the actuator controller shown in figure 5 and in figure 6 as $\mathbf{H}(\mathbf{q})$. There is one actuator controller for each joint, and it uses the joint velocity reference to generate a current signal to the servo valve. The controller is based on a forward coupling that uses equation (22) and a proportional-integral gain to correct any error left from the forward coupling.

In figure 5 the term $\mathbf{D}(\mathbf{p})$ is the forward coupling term, PI represent the proportional-integral controller and $\mathbf{C}(q)$ is the feedback term.
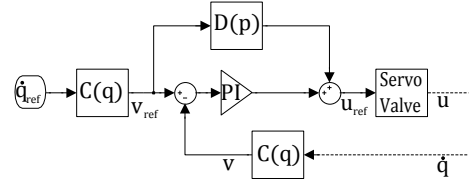

Fig. 5. *Actuator Controller Structure.*

The tool-point controller for the redundant manipulator, in figure 6 shows the complete structure from the tool position and velocity set-points to the manipulator. The fixed constants K_p and K_d are gains for minimizing the error in both position and velocity. The matrix $\mathbf{J}_{\mathbf{W}}^{\dagger}(\mathbf{q})$ is the weighted pseudo inverse term in the first part of (13), while $\mathbf{N}(\mathbf{q})$ represents the Null Space Control, and is the $(\mathbf{I} - \mathbf{J}\mathbf{J}_{\mathbf{W}}^{\dagger})\dot{\mathbf{q}}_0$ term of (13). $\mathbf{H}(\mathbf{q})$ is the actuator regulator and is described in figure 5. $\mathbf{J}(\mathbf{q})$ is the equation in (4) and $\mathbf{F}(\mathbf{q})$ is the forward kinematic (3)
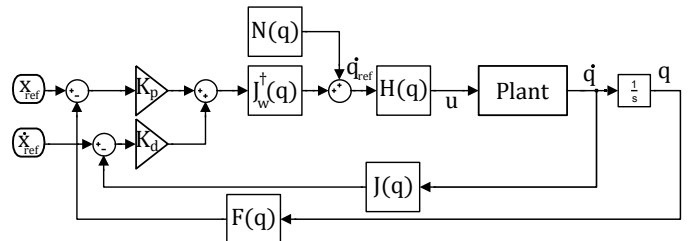

Fig. 6. *Manipulator control structure.*

3. IMPLEMENTATION

The proposed control strategy was implemented both in a simulation model as well as a physical model. The simulation model was experimentally calibrated and, in turn, used to develop and evaluate details in the control strategy.

3.1 Wave Disturbance

In order to test the control strategy the manipulator was arranged in series with a 6-dof Stewart platform that was programmed to emulate wave induced vessel motion. The wave disturbance represented by a Modified Pierson-Moskovitz spectrum is used in both simulations and experiments. It is written as:

$$\mathbf{S}_{\zeta\zeta}(\omega) = \frac{A}{\omega^5} e^{\frac{-B}{\omega^4}} \tag{24}$$

$$A = \frac{172.53 H_{1/3}^2}{\overline{T}^4} \tag{25}$$

$$B = \frac{689.97}{\overline{T}^4} \tag{26}$$

where $H_{1/3}$ is the significant wave height and $\overline{T}$ is the average wave period. Simulation of the sea surface elevation is described in work by Perez (2005) and defined by:

$$\zeta(t) = \sum_{n=1}^{N} \sqrt{2\mathbf{S}_{\zeta\zeta} \cdot \omega_n^* \cdot \Delta\omega} \cdot \cos(\omega_n^* t + \epsilon) \tag{27}$$

$$\omega_n^* = w_n \in [\omega_n - \frac{\Delta\omega}{2}, \omega_n + \frac{\Delta\omega}{2}] \tag{28}$$

where N is the number of wave frequencies, ω_n is chosen by fixed steps of $\Delta\omega$ that is the step between the two frequencies $(\omega_{(n+1)} - \omega_n)$, ω_n^* is the n-th frequency and is chosen randomly in its domain defined in (28), t is time and ϵ is the phase.

Using (27), a time series of the sea surface elevation or heave motion is created. It is shown in figure 7. Since the wave amplitude of the time series is greater than the capability range for heave motion of the Stewart platform and hydraulic manipulator, it has to be downscaled. To introduce an additional disturbance, a pitch motion time series was generated by scaling the time derivative of the wave elevation, thereby emulating the tangent of the wave.

The time domain simulation of the redundant manipulator is done using the commercial modeling software `SimulationX`® and `MATLAB/Simulink`®, where the latter is used for the weighted pseudo-inverse control.

3.2 Experimental Setup

The experimental setup contains the redundant hydraulic manipulator and a Stewart platform. The Stewart platform has a parallel kinematic structure that consists of two platforms connected by six actuated legs. One of the platforms are fixed to the ground, while the other platform has the ability to move in six-degrees of freedom. As a closed mechanical chain the Stewart platform can manipulate payload with markedly higher mass than itself in a fast and precise manner. These abilities makes the Stewart platform ideal for evaluation and testing the redundant hydraulic manipulator. The goal of the experiments are both
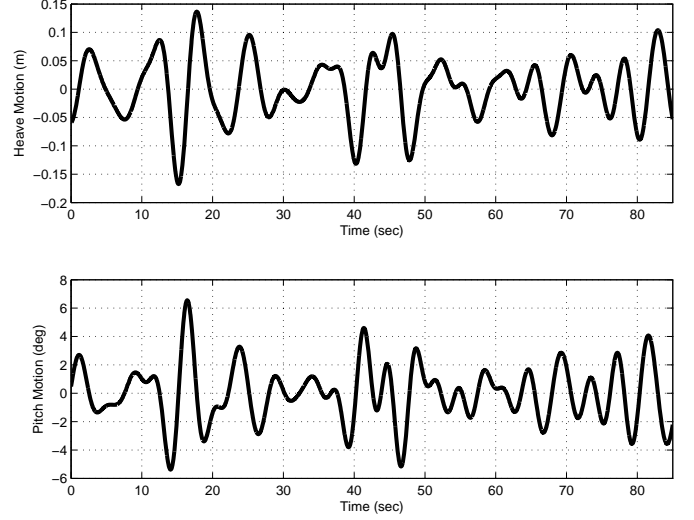

Fig. 7. *Wave motion pattern in $h_b(t)\,(m)$ and $\varphi_b(t)$ (deg).*

to verify the controller and to get experimental results that can be used for model calibration. The experimental result will contain measurements of the control signals, joint position and oil pressures for each hydraulic cylinder. The physical dimentions for the hydraulic manipulator is listed in the following table:

Link Length		Joint Limit			
L_1	0.93 [m]	y_1^U	2.7 [rad]	y_3^U	0.2 [m]
L_2	0.88 [m]	y_1^L	1.1 [rad]	y_3^L	0 [m]
R_1	0.28 [m]	y_2^U	2.2 [rad]		
R_2	0.10 [m]	y_2^L	0.98 [rad]		

The experiment are done by putting the redundant manipulator on top of the Stewart platform, see figure 8. The platform will then move in reference to the time series of both heave and pitch. The distance $h_b(t)$ and the angle $\varphi_b(t)$ is the heave and pitch motion respectively.

The absolute coordinates of the tool point is measured by means of a FARO laser tracker that is capable of measuring position in three-dimensional space with an accuracy of 0.049mm.

There exist a wide variety of tool point control tasks related to heave compensation. In the experiments presented in this paper emphasis is on global fixation, i.e., maintaining the tool point fixed in the fixed coordinate system $\mathbf{x}^{(0)}$, see figure 8.

$$\mathbf{x}_{ref} = \mathbf{A}\mathbf{x}_{PA}^{(0)} \tag{29}$$

$$\dot{\mathbf{x}}_{ref} = \dot{\varphi}_b \mathbf{B}\mathbf{x}_{PA}^{(0)} + \mathbf{A}\dot{\mathbf{x}}_{PA}^{(0)} \tag{30}$$

where the transformation matrices are given as:

$$\mathbf{A} = \begin{bmatrix} \cos(\varphi_b) & \sin(\varphi_b) \\ -\sin(\varphi_b) & \cos(\varphi_b) \end{bmatrix} \mathbf{B} = \frac{\partial \mathbf{A}}{\partial \varphi_b} = \begin{bmatrix} \cos(\varphi_b) & \sin(\varphi_b) \\ -\sin(\varphi_b) & \cos(\varphi_b) \end{bmatrix} \tag{31}$$
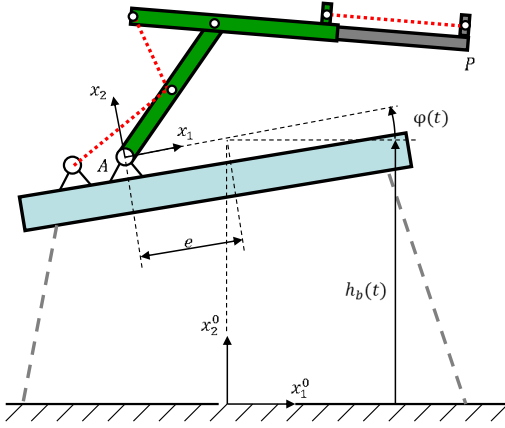
and the global coordinates:

Fig. 8. *Experimental setup with the redundant manipulator and the Stewart platform.*

$$\mathbf{x}_{PA}^{(0)} = \mathbf{x}_P^{(0)} - \mathbf{x}_A^{(0)} = \mathbf{x}_P^{(0)} - \begin{bmatrix} -e\cos(\varphi_b) \\ h_b - e\sin(\varphi_b) \end{bmatrix} \qquad (32)$$

$$\dot{\mathbf{x}}_{PA}^{(0)} = -\dot{\mathbf{x}}_A^{(0)} = -\begin{bmatrix} -e\sin(\varphi_b)\dot{\varphi}_b \\ \dot{h}_b - e\cos(\varphi_b)\dot{\varphi}_b \end{bmatrix} \qquad (33)$$

In the experiments the values for $h_b(t)$, $\dot{h}_b(t)$, $\varphi_b(t)$ and $\dot{\varphi}_b(t)$ are derived from the sensor output of the Stewart platform, i.e., in the same way that a motion reference unit on a vessel would provide the base motion.

In figure 9 and 10 simulated and measured state variables are compared. The accordance is considered satisfactory and easily supports the use of the simulation model to investigate and evaluate control schemes in general. In
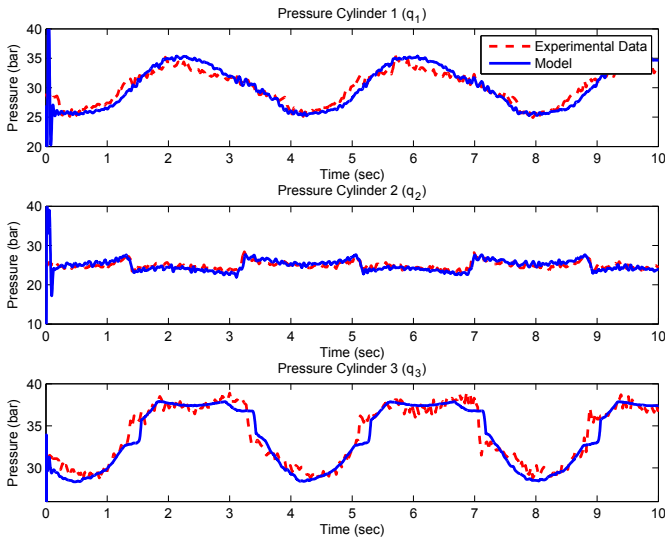

Fig. 9. *Compared result of oil pressures from model and experimental result.*

figure 11 the compensation errors are shown. The result is quite satisfactory and further improvement is propable obtainable by taking into account the combined flexibility of the hydraulic-mechanical manipulator. Also, the null-space control ensures that the actuators move away from end stops and possible saturation, see figure 10.
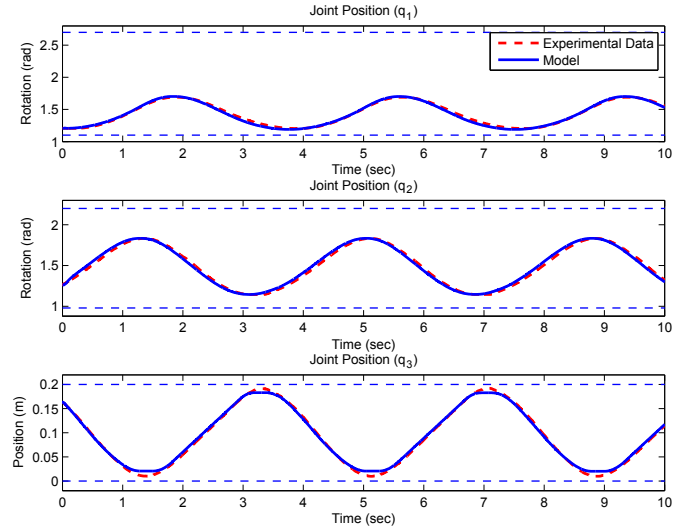
Fig. 10. *Compared result of joint positions from model and experimental result. Horizontal dotted lines represents the mechanical joint saturations*
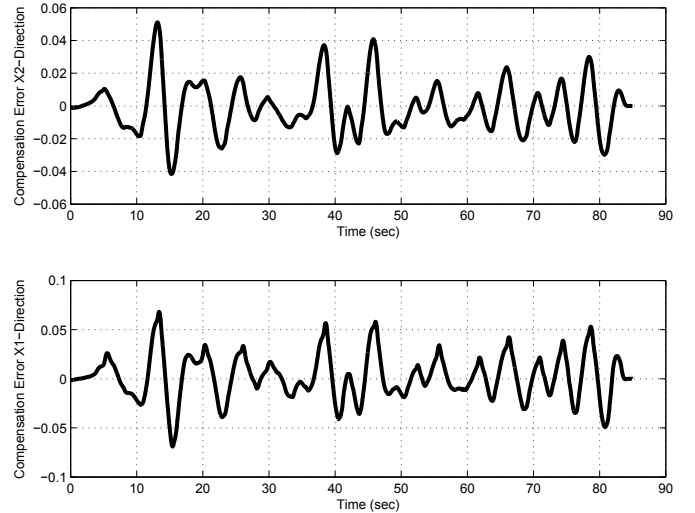

Fig. 11. *Experimental results showing compensation errors in X and Y directions (m).*

4. DISCUSSION AND CONCLUSIONS

In the current work a heave compensation scheme has been developed and implemented both theoretically and practically for a 3-dof redundant hydraulically actuated manipulator. The experimental work has been carried out under dry conditions using a Stewart platform to generate the wave disturbances. The tool-point control scheme has been proved to work satisfactory utilizing a model based feed-forward term that takes into account the nonlinearity of the control valves while avoiding position saturation of the cylinder actuators. Also, it has been possible to obtain a good correlation between measured and simulated data leading to an experimentally calibrated time-domain simulation model that has been used for tuning of the controller parameters.

REFERENCES

Beiner, L. and Mattila (1999). An improved pseudoinverse solution for redundant hydraulic manipulators. *Robotica*, 17, 173–179.

Chan, T.F. and Dubey (1993). Weighted least-norm solution based scheme for avoiding joint limits for redundant manipulators. *Robotics and Automation*, 3, 395–402.

Cinkelj, J., Kamnik, R., Cepon, P., Mihelj, M., and Munih, M. (2010). Robotic control system for hydraulic telescopic handler. In *Robotics in Alpe-Adria-Danube Region (RAAD), 2010 IEEE 19th International Workshop on*, 137 –142. doi:10.1109/RAAD.2010.5524596.

Han, J. and Chung, W.K. (2007). Redundancy resolution for underwater vehicle-manipulator systems with minimizing restoring moments. In *Intelligent Robots and Systems, 2007. IROS 2007. IEEE/RSJ International Conference on*, 3522 –3527. doi: 10.1109/IROS.2007.4399292.

Kucuk, S. and Bingul, Z. (2004). The inverse kinematics solutions of industrial robot manipulators. In *Mechatronics, 2004. ICM '04. Proceedings of the IEEE International Conference on*, 274 – 279. doi: 10.1109/ICMECH.2004.1364451.

Ligeois, A. (1977). Automatic supervisory control of the configuration and behavior of multibody mechanisms. *IEEE Trans. Systems Man Cybernet*, 7, 868–871.

Park, J., Choi, Y., Chung, W.K., and Youm, Y. (2001). Multiple tasks kinematics using weighted pseudo-inverse for kinematically redundant manipulators. In *Robotics and Automation, 2001. Proceedings 2001 ICRA. IEEE International Conference on*, volume 4, 4041 – 4047 vol.4. doi:10.1109/ROBOT.2001.933249.

Pedersen, M.M., Hansen, M.R., and Ballebye, M. (2010). Developing a Tool Point Control Scheme for a Hydraulic Crane Using Interactive Real-time Dynamic Simulation. *Modeling, Identification and Control*, 31(4), 133–143. doi:10.4173/mic.2010.4.2.

Perez, T. (2005). Course keeping and roll reduction using rudder and fins, advances in industrial control. In *Ship motion control:*. London: Springer.

Siciliano, B. (1990). Kinematic control of redundant robot manipulators: A tutorial. *Journal of lntelligent and Robotic Systems*, 3, 201–212.

Whitney, D.E. (1969). Resolved motion rate control of manipulators and human prostheses. *IEEE Trans. Man-Machine Systems*, 10, 47–53.